Article:
Jenkins, E.V., Dharmaprani, D., Schopp, M. et al. (2023) Markov modeling of phase singularity interaction effects in human atrial and ventricular fibrillation. Chaos: An Interdisciplinary Journal of Nonlinear Science, 33 (6). 063136. ISSN: 1054-1500

https://doi.org/10.1063/5.0141890

Chaos
An Interdisciplinary Journal of Nonlinear Science

RESEARCH ARTICLE | JUNE 12 2023

Markov modeling of phase singularity interaction effects in human atrial and ventricular fibrillation

Evan V. Jenkins ; Dhani Dharmaprani ; Madeline Schopp ; Jing Xian Quah ; Kathryn Tiver ; Lewis Mitchell ; Martyn P. Nash ; Richard H. Clayton ; Kenneth Pope ; Anand N. Ganesan

Chaos 33, 063136 (2023)
https://doi.org/10.1063/5.0141890

Markov modeling of phase singularity interaction effects in human atrial and ventricular fibrillation

Cite as: Chaos 33, 063136 (2023); doi: 10.1063/5.0141890
Submitted: 9 January 2023 · Accepted: 12 May 2023 ·
Published Online: 12 June 2023

Evan V. Jenkins,[1] Dhani Dharmaprani,[1,2] Madeline Schopp,[2] Jing Xian Quah,[1,3] Kathryn Tiver,[3] Lewis Mitchell,[4] Martyn P. Nash,[5] Richard H. Clayton,[6] Kenneth Pope,[2] and Anand N. Ganesan[1,3,a)]

AFFILIATIONS

[1]College of Medicine and Public Health, Flinders University, Adelaide 5042, Australia
[2]College of Science and Engineering, Flinders University, Adelaide 5042, Australia
[3]Department of Cardiovascular Medicine, Flinders Medical Centre, Adelaide 5042, Australia
[4]School of Mathematical Sciences, University of Adelaide, Adelaide 5005, Australia
[5]Auckland Bioengineering Institute, University of Auckland, Auckland 1010, New Zealand
[6]Insigneo Institute for In Silico Medicine and Department of Computer Science, University of Sheffield, Sheffield, S1 4DP, United Kingdom

[a)]**Author to whom correspondence should be addressed:** anand.ganesan@flinders.edu.au

ABSTRACT

Atrial and ventricular fibrillation (AF/VF) are characterized by the repetitive regeneration of topological defects known as phase singularities (PSs). The effect of PS interactions has not been previously studied in human AF and VF. We hypothesized that PS population size would influence the rate of PS formation and destruction in human AF and VF, due to increased inter-defect interaction. PS population statistics were studied in computational simulations (Aliev–Panfilov), human AF and human VF. The influence of inter-PS interactions was evaluated by comparison between directly modeled discrete-time Markov chain (DTMC) transition matrices of the PS population changes, and M/M/∞ birth-death transition matrices of PS dynamics, which assumes that PS formations and destructions are effectively statistically independent events. Across all systems examined, PS population changes differed from those expected with M/M/∞. In human AF and VF, the formation rates decreased slightly with PS population when modeled with the DTMC, compared with the static formation rate expected through M/M/∞, suggesting new formations were being inhibited. In human AF and VF, the destruction rates increased with PS population for both models, with the DTMC rate increase exceeding the M/M/∞ estimates, indicating that PS were being destroyed faster as the PS population grew. In human AF and VF, the change in PS formation and destruction rates as the population increased differed between the two models. This indicates that the presence of additional PS influenced the likelihood of new PS formation and destruction, consistent with the notion of self-inhibitory inter-PS interactions.

A characteristic observation in human atrial and ventricular fibrillation is the repetitive formation and destruction of topological defects known as phase singularities (PSs). These defects, also known as rotors, are considered to be important in the maintenance of fibrillation. The effect of interactions between defects has been extensively studied in theoretical literature and in studies of non-cardiac systems of defect mediated turbulence but has not been previously studied in human atrial and ventricular fibrillation. In this study, we examine the interaction between PS, and whether increased population size influences PS formation and destruction rates, assessed through Markov modeling of the PS dynamics. This is performed in (1) computational simulations (Aliev–Panfilov model), (2) human AF collected using 64 electrode intracardiac basket catheters, and (3) human VF collected using 256 electrode epicardial socks placed around the ventricle prior to cardiac surgery. In this study, we find evidence of a self-inhibitory effect on PS formations and destructions as the PS population increases.

I. INTRODUCTION

The repetitive creation and annihilation of spiral vortices is a recurrent motif in spatiotemporally turbulent nonequilibrium systems,[1,2] occurring in numerous physical,[3–5] chemical,[6,7] and

biological settings.[8,9] A characteristic property of spiral vortices is the presence of topological defects known as phase singularities (PSs) at their pivoting region, leading to the characterization of this form of turbulence as defect-mediated turbulence or spiral defect chaos.[10] This form of turbulence has been identified and studied across a wide range of physical, experimental, and theoretical settings. Examples include the regeneration of spiral vortices in Reyleigh–Bernard convection,[4,11–13] theoretical studies investigating their population dynamics in the complex Ginzberg–Landau equation,[10,14,15] and biological settings such as electrical waves within the brain,[16,17] or Rho-GTP diffusion in the membrane of cells.[9]

The continuous formation and destruction of spiral vortices may also be clinically relevant in the context of cardiac fibrillation.[18] Fibrillation is a disorganized aperiodic arrhythmia that occur in the atrium or ventricle. Fibrillation is characterized by the continuous regeneration of spiral vortices (in 2D) or scroll waves (their 3D counterpart).[19–21] The statistical properties of PS formation and destruction in human atrial and ventricular fibrillation (AF/VF) have recently been studied.[19–22] Those investigations suggested PS lifetimes and inter-formation times could be modeled as renewal processes.[21] It was further demonstrated that by combining rate constants of PS formation and destruction in an M/M/∞ birth-death process, PS population dynamics such as the number of PS and the probability distribution of PS population size could be modeled under a Poisson distribution in human AF and VF.[18–20]

In so doing, these statistical findings in human cardiac fibrillation were consistent with theoretical predictions of PS dynamics based on an assumption of statistical independence between the lifetimes and inter-formation times of all PS.[14,23] The assumption of statistical independence that was used to generate these distributions has also been implied in experimental studies of topological defect dynamics in a range of experimental settings with comparable spiral defect chaos.[6,9,11–13] These studies have collectively shown: (i) PS lifetimes may be modeled with an exponential distribution[9,21,24] and (ii) PS population dynamics may be modeled with a Poisson distribution.[6,11–13] The Poisson distribution can be seen to be the steady state distribution arising as a consequence of an M/M/∞ birth-death process.[25]

An intrinsic assumption of the Poisson distribution is that nucleation and destruction events for PS are effectively statistically independent. However, in these systems, PS are in fact topologically connected by isophasic lines,[26] and, therefore, potentially subject to inter-PS interactions. In this study, we hypothesized that this interaction effect between PS could be quantified by careful analysis of the directly modeled transition matrix for the different PS population levels (n). We reasoned that through comparison of the difference between the directly modeled Markov transition matrix and the $M/M/\infty$ birth–death transition matrix which assumes each PS is effectively statistically independent of each other, we could quantify the effect of interactions between PS on the formation and destruction process. Previously, a Markov transition matrix has been proposed theoretically by Aron *et al.* but to date there have not been studies using Markov modeling of PS dynamics in human AF and VF data.[27]

This was performed in three stages. We first examine the effect of Markov modeling of PS transition dynamics in the Aliev–Panfilov model of spiral defect chaos.[28,29] By considering the differences between two Markov models, (1) a discrete-time Markov chain (DTMC) transition matrix that directly represents observed PS population dynamics and (2) a M/M/∞ birth–death transition matrix, we aimed to investigate the effect of inter-phase singularity interaction on PS population dynamics. We then apply the same approach to examine inter-phase singularity interaction in human AF mapped with basket catheter recordings, and human VF mapped with epicardial sock electrodes at cardiac surgery.

II. METHODS

The methods are presented in the following sections. Section I deals with the Aliev–Panfilov model, and approach to data acquisition in human AF and VF. Section II deals with the methods for signal pre-processing, phase singularity detection, and tracking in each of the systems studied. Section III deals with the statistical modeling of phase singularity population dynamics, comparing the direct Markov modeling approach to the M/M/∞ approach to determine PS population interaction effects. Figure 1 provides an overview on the modeling approaches utilized in this study.

A. Section 1—Model and data acquisition

1. Aliev–Panfilov model of spiral defect chaos

To provide initial theoretical insight into the Markov modeling approach, we first examined the Aliev–Panfilov (APV) mode cell model of spiral defect chaos.[29] The APV model is a simple model of cardiac excitation, developed as an extension of the FitzHugh–Nagumo model, so that it adequately modeled the dynamics of pulse propagation in the myocardium.[29,30] The model is described by the following equations:

$$\frac{\partial e}{\partial t} = -ke(e-a)(e-1) - er + D\Delta_2 e + \cdots, \tag{1}$$

$$\frac{\partial r}{\partial t} = \left[\epsilon + \frac{\mu_1 r}{\mu_2 + e}\right][-r - ke(e-b-1)]\cdots. \tag{2}$$

In these equations, e describes the transmembrane potential, D is the diffusion coefficient, Δ_2 is the Laplacian operator ($\Delta_2 = \frac{\partial^2}{\partial x^2} + \frac{\partial^2}{\partial y^2}$), and r is the conductance of the slow inward current.[29]

To establish spiral defect chaos, the model parameters established were $a = 0.1$, $\mu_2 = 0.3$, $k = 8$, $\epsilon = 0.01$, and $b = 0.1$.[29] The parameter μ_1 controls the steepness of the action potential restitution curve across the two-dimensional square grid (which in this case was $N \times N = 200 \times 200$ nodes). Random variation of $\mu 1$ was achieved by using MATLAB's pseudorandom number generator to assign a value in each model between 0.01 and 0.1, simulating inhomogeneous AF substrate (supplementary material, S1). This leads to unique simulations of spiral waves with areas of high dynamical instability that are surrounded by dynamically stable areas, as observed during human AF and VF. To simulate the annihilation of electrical waves as they propagate into the atrial or ventricular walls, no flux boundary conditions were imposed. The model was also run with a forward-Euler time integration step of 0.02 ms and a space integration step of 0.6 mm, as had been utilized in previous studies of the model.[29,31]

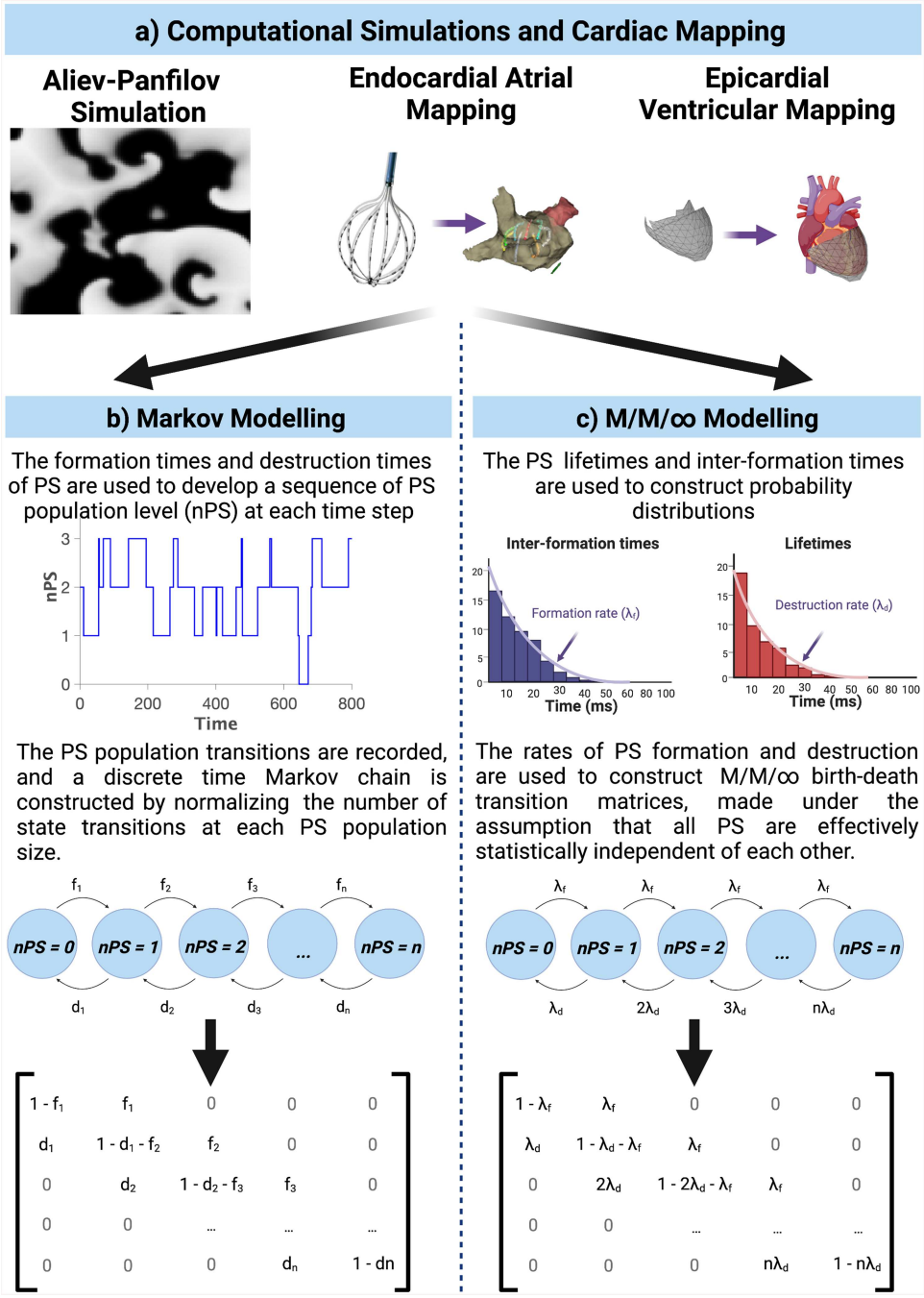

FIG. 1. Overview of modeling approaches utilized in this study. (a) An overview of the simulation data and human data collection. (b) An overview of the discrete time Markov chain modeling approach. (c) An overview of the M/M/∞ modeling approach.

These simulations were performed for 80 000 time steps (1600 ms). For the purposes of this study, only the period between 30 000 (600 ms) and 80 000 (1600 ms) time steps was examined in each simulation to avoid the initialization phase (which does not reflect human AF and VF spiral wave dynamics). During this phase, a single spatially anchored spiral wave is generated, which gradually evolves into a turbulent system of multiple non-stationary spiral waves propagating throughout the grid. In total, N = 40 simulations were generated.

2. Human AF recordings

Human AF data were collected as described in previous studies.[19,21] 64-electrode basket catheters were used to map the atria

[Constellation, Boston Scientific, 48 mm (4 mm spacing), 60 mm (5 mm spacing)]. Unipolar electrogram recordings were obtained from patients prior to AF ablation [0.5–500 Hz, 2000 Hz sampling frequency]. Ethics approval was obtained (IRB Approval No. 110634). 29 epochs of AF were analyzed (n = 9 patients). Patient characteristics are detailed in Sec. S1 in the supplementary material.

3. Human VF recordings

The human VF data were collected from patients undergoing cardiac surgery as described in previously published studies.[32] A 256-electrode epicardial sock was placed around the ventricle, and VF was induced by electrical stimulation after cross-clamping the aorta. Unipolar electrogram signals were recorded [1000 Hz sampling frequency] with a UneMap recording system. Ethics approval was obtained (IRB Approval No. REC 01/0130). Patient characteristics are detailed in Sec. S1 in the supplementary material. 30 s epochs were examined in this study (n = 8 patients), with three temporally separated stages of VF, (i) perfusion, (ii) ischemia, and (iii) reflow.

B. Section 2—Signal pre-processing and phase singularity detection

1. Signal pre-processing in human AF and VF data

Signal pre-processing was utilized for human AF and VF data in which unipolar electrograms were recorded. Pre-processing was not required in the APV model data which directly simulates transmembrane voltage. For the human AF data, baseline drift was removed from signals by removing the best straight-fit line (detrending). A template subtraction method was used to remove far field ventricular depolarization as described previously,[33] following baseline correction of each epoch. Further pre-processing was applied using a third order Butterworth fitted with a 40–250 Hz bandpass filter, and an eighth order Butterworth filter fitted with 10 Hz low-pass filter applied in forward and reverse modes.[21,34] Pre-processing is further detailed in supplementary material S2a.

In the human VF data, electrode coordinates were projected on a 2D plane. The three-dimensional co-ordinates of mesh vertices were mapped onto a 2D polar plot using a cone-shaped surface projection and Delaunay triangulation.[32] Using this 2D projection, electrode potentials were linearly interpolated from the electrodes onto a fine regular grid (100 × 100 grid points). To remove electrodes possessing poor signal-to-noise ratios, these electrograms were removed from the analyses prior to 2D projection of the mesh by selecting only signals with a dominant frequency within the 1.5 45 Hz band for analyses.[32] Pre-processing is further detailed in supplementary material S2b.

2. Phase singularity detection and tracking

Instantaneous phase for each electrogram was reconstructed by applying the Hilbert transform to the transmembrane voltage in the Aliev Panfilov model, and on the cleaned and pre-processed signal for intracardiac unipolar EGM,[35,36] in human AF and VF data. After applying the Hilbert transform, the instantaneous phase was interpolated using complex vector interpolation to avoid incorrect phase calculation.[37,38] Further details about the phase reconstruction is provided in supplementary material S3a.

A convolution kernel method to detect PS was utilized, which approximates the gradient of phase from the discretized phase map using a finite difference operation in the x and y directions.[32,35] In order to track PS, a tracking algorithm was implemented as previously described.[19–21] New PS were defined as the detection of a PS not falling within the surrounding radius of r of an existing PS for a duration of τ of prior frames. As default, τ was set to 10 ms (20 frames) and r set to 6 in the APV model, 4 in basket AF, and 20 in human VF to account for the varying spatial resolution of the mapped field. PS lifetimes and inter-formation timings were calculated using a look-up table approach. Using the sequence of inter-formation timings and lifetimes, the renewal rate constants for formation (λ_f) and destruction (λ_d) were derived as described in previous studies.[19–21] The approach for detecting and tracking PS is detailed further in supplementary material S3.

C. Section 3—Approach to modeling PS transition dynamics

The objective of the current manuscript was to compare and contrast two statistical approaches to modeling PS transition dynamics: (i) Direct Markov transition matrix modeling [Eq. (3)], and (ii) M/M/∞ modeling [Eq. (4)]. An introduction to the two types of transition matrix used in the study is provided in Fig. 1.

1. Direct Markov model

To model a direct Markovian transition process, a continuous sequence of PS population (n) at each time step was constructed ($nPS_{(t)}$). $nPS_{(t)}$ was created through the use of the formation and destruction times of each PS was used to create a continuous sequence of PS population, increasing each time a new formation occurred during a given time step (t), and decreasing when a PS disappeared. The change between $nPS_{(t)} - nPS_{(t+1)}$ was used to develop a matrix of empirical counts of transitions at each n, which was then normalized into transition probabilities of an increase in population or a decrease in population in a Markovian transition matrix, the discrete-time Markov chain (DTMC), as shown in Eq. (3). The formation rates (f_n), and the destruction rates (d_n) were acquired as the respective transition probabilities at each level of n (where n is the PS current population, starting from 0, $n = i - 1$). $P_{i,j}$ is the transition matrix with column position specified by j, and row position specified by i,

$$P_{i,j} = \begin{bmatrix} 1-f_0 & f_0 & 0 & 0 \\ d_1 & 1-f_1-d_1 & f_1 & 0 \\ 0 & d_2 & 1-f_2-d_2 & f_2 \\ 0 & 0 & d_3 & 1-f_3-d_3 \\ 0 & 0 & 0 & \vdots \end{bmatrix} \cdots . \quad (3)$$

As the probabilities of formation and destruction are formulated by normalizing across all counts at a given level of n, each recording needed to remain at or transition out of a given value of n for a minimum of at least 15 time steps across a full epoch.

2. M/M/∞ model

The direct Markov transition matrix was contrasted with an $M/M/\infty$ birth death transition matrix. An $M/M/\infty$ birth–death process is a continuous-time Markov chain, where new events have Markovian rates of arrivals/formations and destruction.[19,20] As with the direct Markov model, in the $M/M/\infty$ birth–death process, the transition matrix ($P_{i,j}$) [Eq. (4)] the formation rates (f_n), and the destruction rates (d_n) were acquired from the renewal rate constants λ_f (for the formation probability f_i) and λ_d (for the destruction probability d_i) adjusted to represent the transition probabilities at each level of n (where n is the current PS population, starting from 0, $n = i - 1$). $P_{i,j}$ is the transition matrix with column position specified by j, and row position specified by i,

$$P_{i,j} = \begin{bmatrix} 1-\lambda_f & \lambda_f & 0 & 0 \\ \lambda_d & 1-\lambda_f-\lambda_d & \lambda_f & 0 \\ 0 & 2\lambda_d & 1-\lambda_f-2\lambda_d & \lambda_f \\ 0 & 0 & 3\lambda_d & 1-\lambda_f-3\lambda_d \\ 0 & 0 & 0 & \vdots \end{bmatrix} \cdots . \tag{4}$$

D. Statistical analysis

The fundamental research question of this paper is the interaction effect at each of level of PS population on the transition statistics between different PS population levels. To determine this, the following statistical modeling approaches were utilized: (i) linear regression—in the case of the discrete time Markov and M/M/∞ matrices, the transition rate constants for formation and destruction events were separately modeled as dependent variables, and the PS population was considered as the primary predictor. The difference between the predicted regression estimates of the DTMC matrix and M/M/∞ matrix was considered as the interaction effect in each epoch studied. Overall statistics of these estimates were computed for each of the modeled systems studied.

III. RESULTS

A. Interaction of PS in computational simulations

In APV computation simulations, as the PS population increased, the formation rates decreased through the DTMC modeling, as shown in Table I and Fig. 2. This contrasted with the constant formation rate predicted through the $M/M/\infty$ modeling. The p-value for all β estimate was less than 0.05 and is presented along with an expanded table in Sec. 5a in the supplementary material.

TABLE I. Slope (β) of linear regression for the formation and destruction rates between the direct Markov model and $M/M/\infty$ models for the APV computational simulation data.

	β estimate (%/ms)
DTMC formation	−1.08
DTMC destruction	1.78
$M/M/\infty$ destruction	2.00

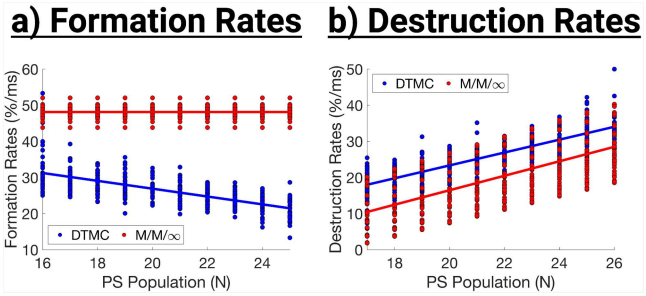

FIG. 2. (a) PS formation rates at different PS population sizes in APV computational simulations. (b) PS destruction rates at different PS population sizes in APV computational simulations.

The destruction rates increased for both the DTMC model and the $M/M/\infty$ model with a positive slope, as shown in Table I and Fig. 2. As the $M/M/\infty$ model possesses as a slope of zero by construction, linear regression was not performed on it for any of the examined systems. The PS formation matrices were restricted to be between 16PS and 25PS, and the PS destruction matrices were restricted to be between 17PS and 26PS.

B. Interaction of PS in human AF

In human AF, as the PS population increased, the formation rate for the DTMC model increased, while the formation rate for the $M/M/\infty$ model remained constant, as shown in Fig. 3. Unlike the APV simulations, the PS formation rates of the DTMC model, initially exceeded the predicted value of the $M/M/\infty$, before decreasing to a lower value at higher PS population sizes.

For the PS destruction rates, for the DTMC model, the destruction rates initially were slower than those of the $M/M/\infty$ model, however as the PS population size increased, the DTMC destruction rates increased, eventually exceeding the $M/M/\infty$ predicted rates, as shown in Fig. 3 and Table II. The p-value for all β estimate was less than 0.05 and is presented along with an expanded table in Sec. 5b in the supplementary material. The PS formation matrices

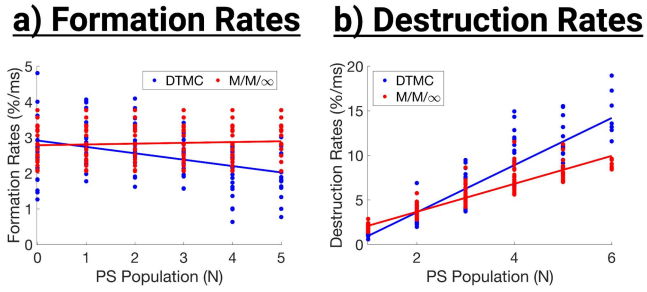

FIG. 3. (a) PS formation rates at different PS populations sizes in human AF mapped using basket catheters. (b) PS destruction rates at different PS population sizes in human AF mapped using basket catheters.

TABLE II. Slope (β)of linear regression for the formation and destruction rates between the direct Markov model and $M/M/\infty$ models for Human AF.

	β estimate (%/ms)
DTMC formation	−0.179
DTMC destruction	2.65
$M/M/\infty$ destruction	1.57

were restricted to be between 0PS and 5PS, and the PS destruction matrices were restricted to be between 1PS and 6PS.

C. Interaction of PS as human VF progresses

The PS population state transitions were next examined in human VF, separated into different stage temporally, (i) Perfusion, (ii) Ischemia, and (iii) Reflow. Across all stages, the DTMC transitions rates differed from the $M/M/\infty$ framework. PS formation rates presented a negative slope as the PS population increased, indicating a decrease in likelihood of new PS formations, shown in Fig. 4 and Table III.

For both the DTMC model and the $M/M/\infty$ model, there was a clear positive slope in the destruction rates as PS population increased, as shown in Fig. 4 and Table III. The formation rates of the DTMC model at lower PS populations exceeded the predicted rate of the $M/M/\infty$ model; however, they decreased below the $M/M/\infty$ predictions as the PS population increased. The destruction rates of the DTMC model gradually exceeded those predicted by the $M/M/\infty$ model as the PS population increased, consistent with the findings in human AF. The p-value for all β estimate was less than 0.05 and is presented along with an expanded table in Sec. 5c in the supplementary material. Across all stages, the PS formation matrices were restricted to between 0PS and 3PS, and the PS destruction matrices were restricted to between 1PS and 4PS.

TABLE III. Slope (β) Linear regression outputs for the formation and destruction rates between the direct Markov model and $M/M/\infty$ models for human VF.

	β estimate (% / ms)
Perfusion	
DTMC formation	−1.02
DTMC destruction	3.42
$M/M/\infty$ destruction	0.970
Ischemia	
DTMC formation	−1.49
DTMC destruction	2.99
$M/M/\infty$ destruction	0.980
Reflow	
DTMC formation	−1.37
DTMC destruction	3.43
$M/M/\infty$ destruction	1.03

IV. DISCUSSION

Although the statistical properties of phase singularity (PS) population dynamics has received extensive study in a wide range of systems,[9,11–15] to date, there have been relatively few studies performed of defect dynamics in human AF and VF.[19,20] In human AF and VF, the rates of PS formation and destruction were of similar average behavior for both the DTMC and $M/M/\infty$ models, however the specific values differed at different PS population sizes. At lower PS populations in AF and VF, the rates of formation for the DTMC model exceeded the values predicted by the $M/M/\infty$ model (Figs. 3 and 4). Similarly, the rates of PS destruction for the DTMC model were less than the predicted rate of the $M/M/\infty$ model (Figs. 3 and 4). As the PS population size increased, this pattern reversed with the DTMC formation rates continuously decreasing below the $M/M/\infty$ model, while the destruction rates of the DTMC began to increase beyond the predictions of the $M/M/\infty$ model (Figs. 3 and 4). In VF, similar rates of PS formation and destruction were observed across the three stages examined, suggesting that the degree of inter-PS interaction does not noticeably change as VF progress. Collectively, these observations may suggest that the systems could trend toward a set value or range for the number of PS active at a given time.

This tendency toward a statistically stable average population size would indicate that large numbers of PS could potentially have an inhibitory effect on new PS formations while encouraging destruction of existing PS. Similarly, as the number of PS decrease, the nature of the system may facilitate increased likelihood of PS formation. These observations could be explained by an increased inhibitory effect imposed by the system as the population increases. This is explanation seems likely, when considering AF and VF as a form of spiral defect chaos. The population dynamics of spiral waves is a well-studied phenomena in studies of such systems.[15,16]

The interaction of stable spirals in excitable media has been extensively studied, including the paired annihilation of PS with opposite chirality and the formation of "multi-armed" spiral/scroll waves from interaction between like chirality vortices.[31,39–41] In these systems, interactions between PS are often a primary cause of PS destruction, including annihilation of weaker vortices, paired annihilation,[39] along with wave break up or collisions with boundaries.[24]

One property of the system that may influence the inhibition of new PS formations is the available space within the system. In comparison to the human AF and VF data, the APV computational simulations contained a far greater number of actively detectable PS. Through visual comparison of the computational simulations and the biological systems (Fig. 5), it can be seen that within the APV simulations, there are far more PS and free wavelets propagating in the system than in the datasets collected from human atria and ventricles. This could be attributed to the larger spatial size of the simulations in comparison to the biological data.

In experimental studies, it has been shown that PS exerts some degree of control over their local domains. In a study by Gray *et al.*, they induced ventricular fibrillation in rabbits and sheep, and observed that on average a rotors/PS would occupy approximately $12 \pm 4\,\text{cm}^2$.[26] From this, they estimated that the total number of rotors in rabbits would be 1–2, 5 for sheep, and then extrapolated this with the surface area in a human heart, to suggest that there

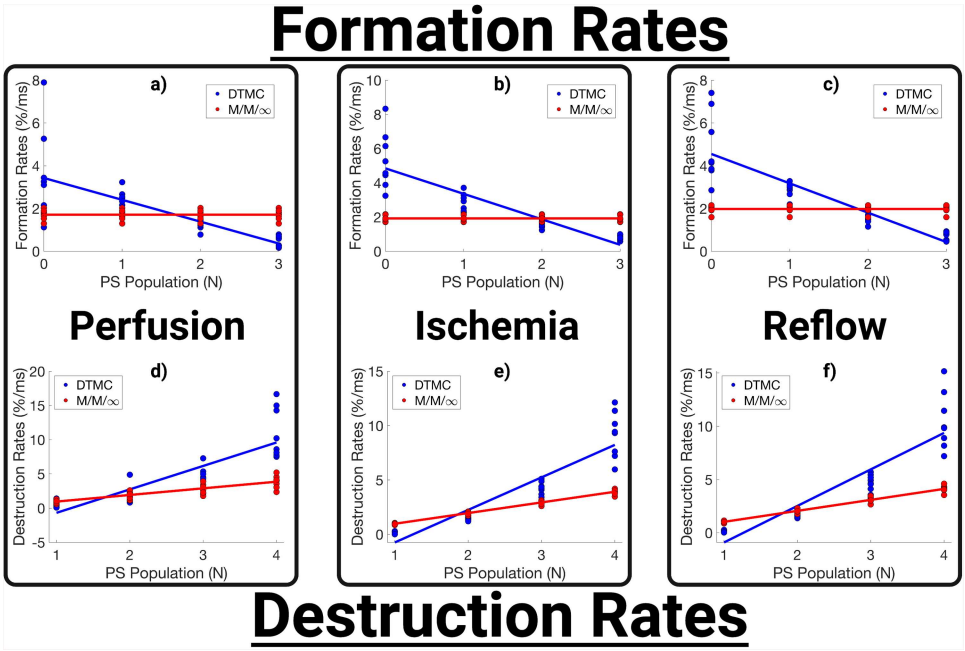

FIG. 4. PS formation rates at different PS population sizes, in distinct stages of VF (a) perfusion, (b) ischemia, (c) reflow. PS destruction rates at different PS population sizes, in distinct stages of VF (d) perfusion, (e) ischemia, (f) reflow.

could be 15 rotors in human AF (although this was made with the assumption that rotor density would be the same in humans). Other studies have suggested that spiral waves occupy finite amounts of space and that the dynamics of that region, known as tiles, are controlled almost entirely by the spiral core/PS.[42]

Another study suggests that the assumption of statistical independence in systems of defect mediated turbulence relies upon the system size.[10] In this study of three-dimensional filaments, they found that as system size decreases, the average surface density of filaments increases. They suggest that this increase in surface filament density increases the likelihood of interaction, with defect pair interactions occurring more strongly. They also postulated that as the system size decreases, the assumption of statistical independence begins to break down due to increased interaction.[10] This observation to date has not been demonstrated in a similar way in human AF and VF data.

Self-inhibition of PS formation in the atria and ventricles could be the result of vortices controlling their local domains, limiting new

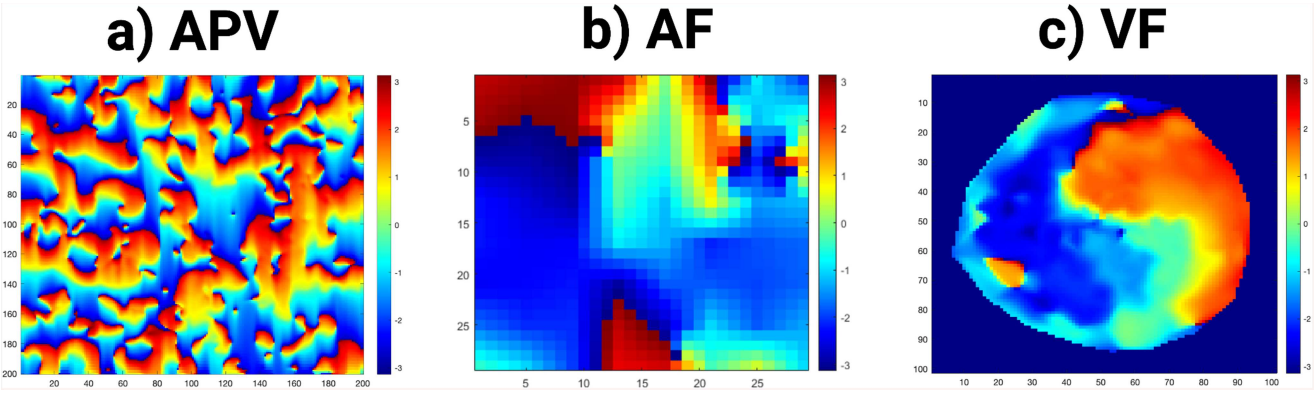

FIG. 5. Phase maps of the examined systems. (a) A phase map of the Aliev–Panfilov computational simulations. (b) A phase map of human AF mapped using basket catheters. (c) A phase map of human VF mapped using epicardial electrode socks.

PS formations in their vicinity as n increases. Each new PS would reduce the amount of available space within the system that is not already controlled by a PS. This could introduce a potential limitation of the assumption of statistical independence between PS, especially at high number of PS relative to the system size, as an inter-PS inhibitory effect would increase with each new PS formation. This inhibitory effect could drive the number of PS down to a semi-stable average number of PS that the system will tend toward. Similar to the $M/M/\infty$ framework previously published,[19,20] this semi-stable system average number of PS would likely be defined by an interplay of system properties governing PS destructions, such as the system space influencing destruction, and the properties of the system which facilitate new PS formations.

In small systems, an inter-PS inhibitory effect could mean that each PS has a significant degree of influence on the overall population dynamics of the system, and similarly that each PS in a large system could very little influence on the overall dynamics of the system.

A. Relationship to previous studies

Our recent studies have examined the statistical properties of spiral waves in AF and VF.[18–21] We first modeled AF as a renewal process,[21] and have since demonstrated that the formation and destruction of PS can be approximated by modeling it as an M/M/∞ birth–death process.[19] We have also demonstrated that these same properties apply in ventricular fibrillation and that the M/M/∞ framework could be used to develop governing equations that explain the PS population dynamics observed in fibrillation.[20] These studies have suggested that the PS population distributions arise from an interplay of PS formation and destruction rates,[19] and that this allows for governing equations to explain the PS population dynamics.[20] The previous studies have been shown to represent the system average behavior quite well.[19–21] However, as shown in this study, around large or small PS populations, the DTMC model provides improved mechanistic understanding.

This study and our previous studies demonstrate that cardiac fibrillation may broadly possess similar properties of other systems of spiral defect mediated turbulence.[18–22] A potential implication of AF/VF demonstrating similar properties to systems of spiral defect mediated turbulence, could be that other properties examined in those systems could potentially apply to cardiac fibrillation.

1. Creation and annihilation in three-dimensional oscillatory media

In a previous study by Davidsen, they postulated that for 3D media, both the creation and annihilation of PS when observed in two-dimensions could be described as linear relationships,[10,15]

$$a(n) = \alpha_1 + \alpha_2 n + \cdots, \tag{5}$$

$$c(n) = \beta_1 + \beta_2 n + \cdots. \tag{6}$$

As cardiac muscle is a 3D structure, it is believed that formation and destruction of spiral vortices observed in 2D experimental recordings reflects 3D filament birth and death,[43–45] which is consistent with our findings in human AF and VF data. The decrease in formation rates and increase in destruction rates for the systems examined in this study can be described by linear equations.

The decrease in formation rate for the AF basket data and VF epicardial sock datasets can be described by a linear equation, as suggested by Davidsen.[10] It also indicates that each PS may exert some influence on the overall dynamics of the system, increasingly inhibiting the formation of new PS as n increases. This could introduce a potential limitation of the assumption of statistical independence between PS, especially at high values of n. The decrease in PS formation rate as n increases may suggest that an inter-PS inhibitory effect could lead to a semi-stable average number of PS, that a system will tend toward. It would also indicate a potential maximum number of PS, as the decreasing rate of PS formation, coupled with the increasing destruction rate, would lead to low probabilities of the system reaching and remaining at high values of n. This inhibition could potentially be driven by the size of the system, as there is finite physical space in the atria, combined with the propensity of larger PS to annihilate smaller PS in their vicinity.

B. Limitations and further work

A number of studies question the efficacy of basket catheter recordings in the study of electrophysiological properties of fibrillation due to technical limitations such as electrode spacing and insufficient contact with the tissue.[38] We acknowledge that these concerns, however by examining human VF recorded using a 256-electrode sock that holistically examined epicardial VF, along with computational simulations of fibrillatory behavior, we show that the same trends occur in other systems and are not a consequence the basket catheter limitations nor are the findings obscured by them.

This work could be expanded upon by examining the formation and destruction rates of PS in three-dimensional models of fibrillation. In particular, models that capture the anatomy and structural complexity of the atria/ventricles could provide further insight into factors that inhibit or facilitate the formation of new PS in humans.

V. CONCLUSION

We have shown that PS in human atrial and ventricular fibrillation share similar statistical properties to those predicted in theoretical models of defect-mediated turbulence. We find that observable PS formation and destruction rates scale linearly with PS population size, a finding demonstrated in humans for the first time, this finding is consistent with contributions from the spiral wave breakup and negative filament tension mechanisms. A self-inhibitory effect of PS population size on PS creation was identified, as well as in mapping data which partially observe systems. Further studies in human cardiac fibrillation of the mechanisms of breakup are required to optimize treatment of these life-threatening conditions.

SUPPLEMENTARY MATERIAL

See the supplementary material for patient characteristics for the human AF and VF data, additional information regarding the signal processing, and additional PS formation and destruction rate data.

ACKNOWLEDGMENTS

This work was supported by the National Health and Medical Research Council of Australia Ideas Grant (No. 2010522) and the National Heart Foundation of Australia (No. 101188).

AUTHOR DECLARATIONS

Conflict of Interest

The authors have no conflicts to disclose.

Ethics Approval

Ethics approval for human AF data was obtained (IRB Approval No. 110634). Ethics approval for human VF data was obtained (IRB Approval No. REC 01/0130).

Author Contributions

Evan V. Jenkins: Conceptualization (equal); Data curation (equal); Formal analysis (equal); Investigation (equal); Methodology (equal); Resources (equal); Software (equal); Validation (equal); Visualization (equal); Writing – original draft (equal); Writing – review & editing (equal). **Dhani Dharmaprani:** Data curation (equal); Resources (equal); Software (equal); Writing – review & editing (equal). **Madeline Schopp:** Software (equal). **Jing Xian Quah:** Writing – review & editing (equal). **Kathryn Tiver:** Data curation (equal); Writing – review & editing (equal). **Lewis Mitchell:** Writing – review & editing (equal). **Martyn P. Nash:** Data curation (equal); Software (equal); Writing – review & editing (equal). **Richard H. Clayton:** Data curation (equal); Software (equal); Writing – review & editing (equal). **Kenneth Pope:** Writing – review & editing (equal). **Anand N. Ganesan:** Conceptualization (equal); Funding acquisition (equal); Methodology (equal); Project administration (equal); Supervision (equal); Writing – original draft (equal); Writing – review & editing (equal).

DATA AVAILABILITY

The data that support the findings of this study are available from the corresponding author upon reasonable request.

REFERENCES

[1]M. Cross and H. Greenside, *Pattern Formation and Dynamics in Nonequilibrium Systems* (Cambridge University Press, 2009).
[2]M. C. Cross and P. C. Hohenberg, "Pattern formation outside of equilibrium," Rev. Mod. Phys. **65**, 851 (1993).
[3]Q. Ouyang and J.-M. Flesselles, "Transition from spirals to defect turbulence driven by a convective instability," Nature **379**, 143–146 (1996).
[4]D. A. Egolf, I. V. Melnikov, W. Pesch, and R. E. Ecke, "Mechanisms of extensive spatiotemporal chaos in Rayleigh–Bénard convection," Nature **404**, 733–736 (2000).
[5]S. W. Morris, E. Bodenschatz, D. S. Cannell, and G. Ahlers, "Spiral defect chaos in large aspect ratio Rayleigh–Bénard convection," Phys. Rev. Lett. **71**, 2026 (1993).
[6]C. Qiao, H. Wang, and Q. Ouyang, "Defect-mediated turbulence in the Belousov–Zhabotinsky reaction," Phys. Rev. E **79**, 016212 (2009).
[7]C. Beta, A. S. Mikhailov, H. H. Rotermund, and G. Ertl, "Defect-mediated turbulence in a catalytic surface reaction," Europhys. Lett. **75**, 868 (2006).
[8]J. Lechleiter, S. Girard, E. Peralta, and D. Clapham, "Spiral calcium wave propagation and annihilation in *Xenopus laevis* oocytes," Science **252**, 123–126 (1991).
[9]T. H. Tan, J. Liu, P. W. Miller, M. Tekant, J. Dunkel, and N. Fakhri, "Topological turbulence in the membrane of a living cell," Nat. Phys. **16**, 657–662 (2020).
[10]J. Davidsen, M. Zhan, and R. Kapral, "Filament-induced surface spiral turbulence in three-dimensional excitable media," Phys. Rev. Lett. **101**, 208302 (2008).
[11]E. Bodenschatz, W. Pesch, and G. Ahlers, "Recent developments in Rayleigh–Bénard convection," Annu. Rev. Fluid Mech. **32**, 709–778 (2000).
[12]R. E. Ecke and Y. Hu, "Spiral defect chaos in Rayleigh-Bénard convection: Defect population statistics," Phys A: Stat. Mech. Appl. **239**, 174–188 (1997).
[13]R. E. Ecke, Y. Hu, R. Mainieri, and G. Ahlers, "Excitation of spirals and chiral symmetry breaking in Rayleigh–Bénard convection," Science **269**, 1704–1707 (1995).
[14]L. Gil, J. Lega, and J. Meunier, "Statistical properties of defect-mediated turbulence," Phys. Rev. A **41**, 1138 (1990).
[15]G. St-Yves and J. Davidsen, "Influence of the medium's dimensionality on defect-mediated turbulence," Phys. Rev. E **91**, 032926 (2015).
[16]X. Huang, W. Xu, J. Liang, K. Takagaki, X. Gao, and J.-Y. Wu, "Spiral wave dynamics in neocortex," Neuron **68**, 978–990 (2010).
[17]J. Viventi, D.-H. Kim, L. Vigeland, E. S. Frechette, J. A. Blanco, Y.-S. Kim, A. E. Avrin, V. R. Tiruvadi, S.-W. Hwang, A. C. Vanleer, D. F. Wulsin, K. Davis, C. E. Gelber, L. Palmer, J. Van Der Spiegel, J. Wu, J. Xiao, Y. Huang, D. Contreras, J. A. Rogers, and B. Litt, "Flexible, foldable, actively multiplexed, high-density electrode array for mapping brain activity *in vivo*," Nat. Neurosci. **14**, 1599–1605 (2011).
[18]E. V. Jenkins, D. Dharmaprani, M. Schopp, J. X. Quah, K. Tiver, L. Mitchell, K. Pope, and A. N. Ganesan, "Understanding the origins of the basic equations of statistical fibrillatory dynamics," Chaos **32**, 032101 (2022).
[19]D. Dharmaprani, E. Jenkins, M. Aguilar, J. X. Quah, A. Lahiri, K. Tiver, L. Mitchell, P. Kuklik, C. Meyer, and S. Willems, "M/M/infinity birth-death processes—A quantitative representational framework to summarize and explain phase singularity and wavelet dynamics in atrial fibrillation," Front. Physiol. **11**, 616866 (2021).
[20]D. Dharmaprani, E. V. Jenkins, J. X. Quah, A. Lahiri, K. Tiver, L. Mitchell, C. P. Bradley, M. Hayward, D. J. Paterson, P. Taggart, R. H. Clayton, M. P. Nash, and A. N. Ganesan, "A governing equation for rotor and wavelet number in human clinical ventricular fibrillation: Implications for sudden cardiac death," Heart Rhythm. **19**, 295–305 (2022).
[21]D. Dharmaprani, M. Schopp, P. Kuklik, D. Chapman, A. Lahiri, L. Dykes, F. Xiong, M. Aguilar, B. Strauss, L. Mitchell, K. Pope, C. Meyer, S. Willems, F. G. Akar, S. Nattel, A. D. McGavigan, and A. N. Ganesan, "Renewal theory as a universal quantitative framework to characterize phase singularity regeneration in mammalian cardiac fibrillation," Circ.: Arrhythmia Electrophysiol. **12**, e007569 (2019).
[22]E. V. Jenkins, D. Dharmaprani, M. Schopp, J. X. Quah, K. Tiver, L. Mitchell, F. Xiong, M. Aguilar, K. Pope, and F. G. Akar, "The inspection paradox: An important consideration in the evaluation of rotor lifetimes in cardiac fibrillation," Front. Physiol. **13**, 920788 (2022).
[23]P. Coullet, L. Gil, and J. Lega, "Defect-mediated turbulence," Phys. Rev. Lett. **62**, 1619 (1989).
[24]T. Lilienkamp, J. Christoph, and U. Parlitz, "Features of chaotic transients in excitable media governed by spiral and scroll waves," Phys. Rev. Lett. **119**, 054101 (2017).
[25]S. M. Ross, *Introduction to Probability Models* (Academic Press, 2014).
[26]R. A. Gray, A. M. Pertsov, and J. Jalife, "Spatial and temporal organization during cardiac fibrillation," Nature **392**, 75–78 (1998).
[27]M. Aron, S. Herzog, U. Parlitz, S. Luther, and T. Lilienkamp, "Spontaneous termination of chaotic spiral wave dynamics in human cardiac ion channel models," PLoS One **14**, e0221401 (2019).
[28]R. R. Aliev and A. V. Panfilov, "Modeling of heart excitation patterns caused by a local inhomogeneity," J. Theor. Biol. **181**, 33–40 (1996).
[29]K. Ten Tusscher and A. Panfilov, "Influence of nonexcitable cells on spiral breakup in two-dimensional and three-dimensional excitable media," Phys. Rev. E **68**, 062902 (2003).

[30]R. R. Aliev and A. V. Panfilov, "A simple two-variable model of cardiac excitation," Chaos, Solitons, Fractals **7**, 293–301 (1996).
[31]C. W. Zemlin, K. Mukund, V. N. Biktashev, and A. M. Pertsov, "Dynamics of bound states of same-chirality spiral waves," Phys. Rev. E **74**, 016207 (2006).
[32]M. P. Nash, A. Mourad, R. H. Clayton, P. M. Sutton, C. P. Bradley, M. Hayward, D. J. Paterson, and P. Taggart, "Evidence for multiple mechanisms in human ventricular fibrillation," Circulation **114**, 536–542 (2006).
[33]S. Shkurovich, A. V. Sahakian, and S. Swiryn, "Detection of atrial activity from high-voltage leads of implantable ventricular defibrillators using a cancellation technique," IEEE Trans. Biomed. Eng. **45**, 229–234 (1998).
[34]C. H. Roney, C. D. Cantwell, N. A. Qureshi, R. A. Chowdhury, E. Dupont, P. B. Lim, E. J. Vigmond, J. H. Tweedy, F. S. Ng, and N. S. Peters, "Rotor tracking using phase of electrograms recorded during atrial fibrillation," Ann. Biomed. Eng. **45**, 910–923 (2017).
[35]M. A. Bray and J. P. Wikswo, "Considerations in phase plane analysis for nonstationary reentrant cardiac behavior," Phys. Rev. E, **65**, 051902 (2002).
[36]P. Kuklik, S. Zeemering, B. Maesen, J. Maessen, H. J. Crijns, S. Verheule, A. N. Ganesan, and U. Schotten, "Reconstruction of instantaneous phase of unipolar atrial contact electrogram using a concept of sinusoidal recomposition and Hilbert transform," IEEE Trans. Biomed. Eng. **62**, 296–302 (2015).
[37]D. Vidmar and W. J. Rappel, "To the editor—On the deformation and interpolation of phase maps," Heart Rhythm **15**, e3 (2018).
[38]C. H. Roney, C. D. Cantwell, J. D. Bayer, N. A. Qureshi, P. B. Lim, J. H. Tweedy, P. Kanagaratnam, N. S. Peters, E. J. Vigmond, and F. S. Ng, "Spatial resolution requirements for accurate identification of drivers of atrial fibrillation," Circ.: Arrhythmia Electrophysiol. **10**, e004899 (2017).
[39]R. M. Zaritski and A. M. Pertsov, "Stable spiral structures and their interaction in two-dimensional excitable media," Phys. Rev. E **66**, 066120 (2002).
[40]R. M. Zaritski, S. F. Mironov, and A. M. Pertsov, "Intermittent self-organization of scroll wave turbulence in three-dimensional excitable media," Phys. Rev. Lett. **92**, 168302 (2004).
[41]C. Zemlin, K. Mukund, M. Wellner, R. Zaritsky, and A. Pertsov, "Asymmetric bound states of spiral pairs in excitable media," Phys. Rev. Lett. **95**, 098302 (2005).
[42]G. Byrne, C. D. Marcotte, and R. O. Grigoriev, "Exact coherent structures and chaotic dynamics in a model of cardiac tissue," Chaos **25**, 033108 (2015).
[43]R. H. Clayton, "Vortex filament dynamics in computational models of ventricular fibrillation in the heart," Chaos **18**, 043127 (2008).
[44]R. H. Clayton, "Influence of cardiac tissue anisotropy on re-entrant activation in computational models of ventricular fibrillation," Phys. D: Nonlinear Phenom. **238**, 951–961 (2009).
[45]R. H. Clayton and A. V. Holden, "Dynamics and interaction of filaments in a computational model of re-entrant ventricular fibrillation," Phys. Med. Biol. **47**, 1777 (2002).